Rope Support System for the Jinping Neutrino Experiment

Beibei Li, Yanjun Tong
Hefei University Of Technology
School Of Civil Engineering

2026.7.4

CONTENTS

1

Background

01 Background

1.1 Applications of high-performance fibre ropes in neutrino detector

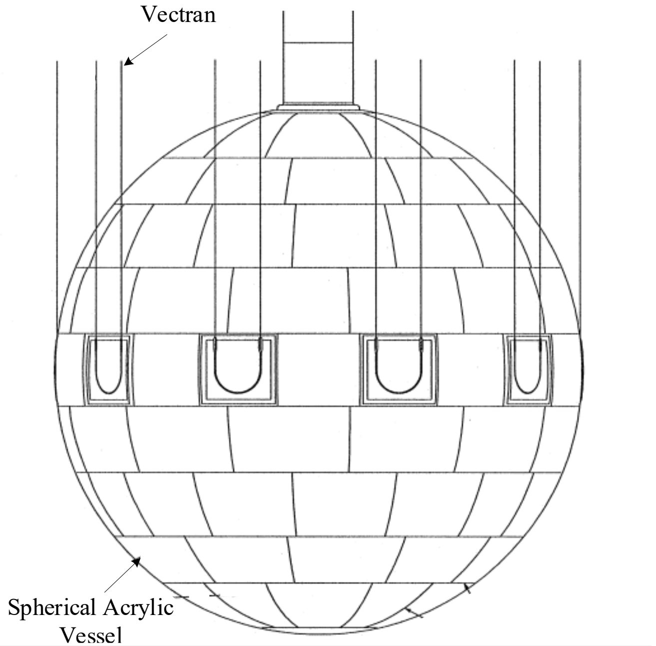

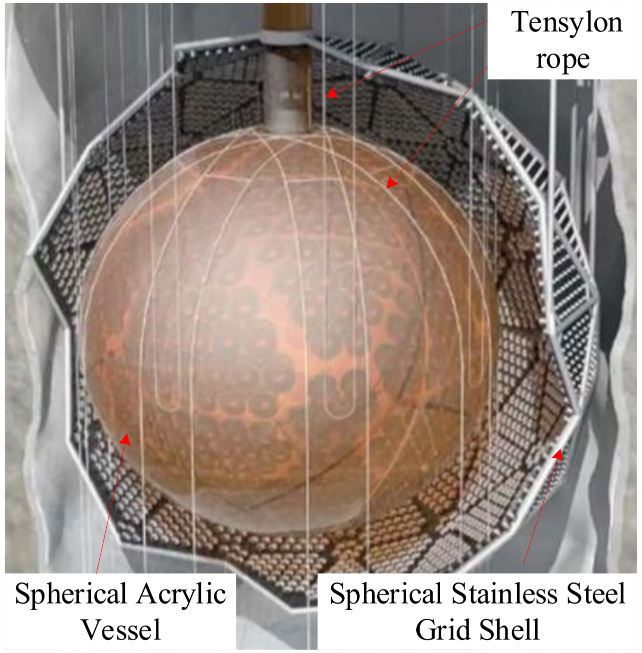

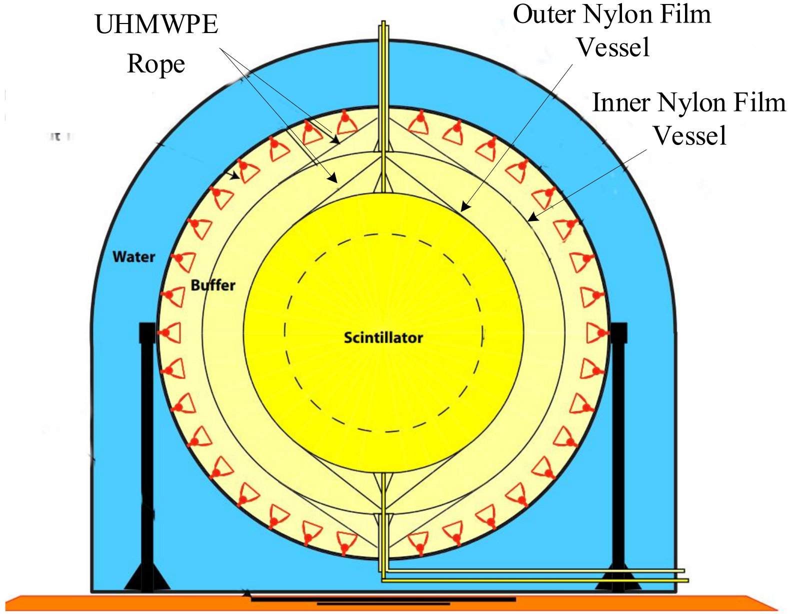

SNO	SNO+	Borexino
Canada	Canada	Italy
Acrylic Vessel + Stainless Steel Grid Shell	Acrylic Vessel + Stainless Steel Grid Shell	Inner and Outer Nylon Film Vessels + Stainless Steel Grid Shell
A 24.4 mm Vectran rope is arranged at the equator to restrain the downward movement of the acrylic vessel.	A 39.6 mm Tensylon rope is wrapped around the top chimney and anchored at the bottom to restrain uplift, while equatorial suspension restrains downward movement.	Ultra-High Molecular Weight Polyethylene ropes restrain the uplift and downward movement of the inner and outer nylon film vessels.

01 Background

➢ 1.2 Jinping Neutrino Experiment and the need for a rope-supported acrylic vessel

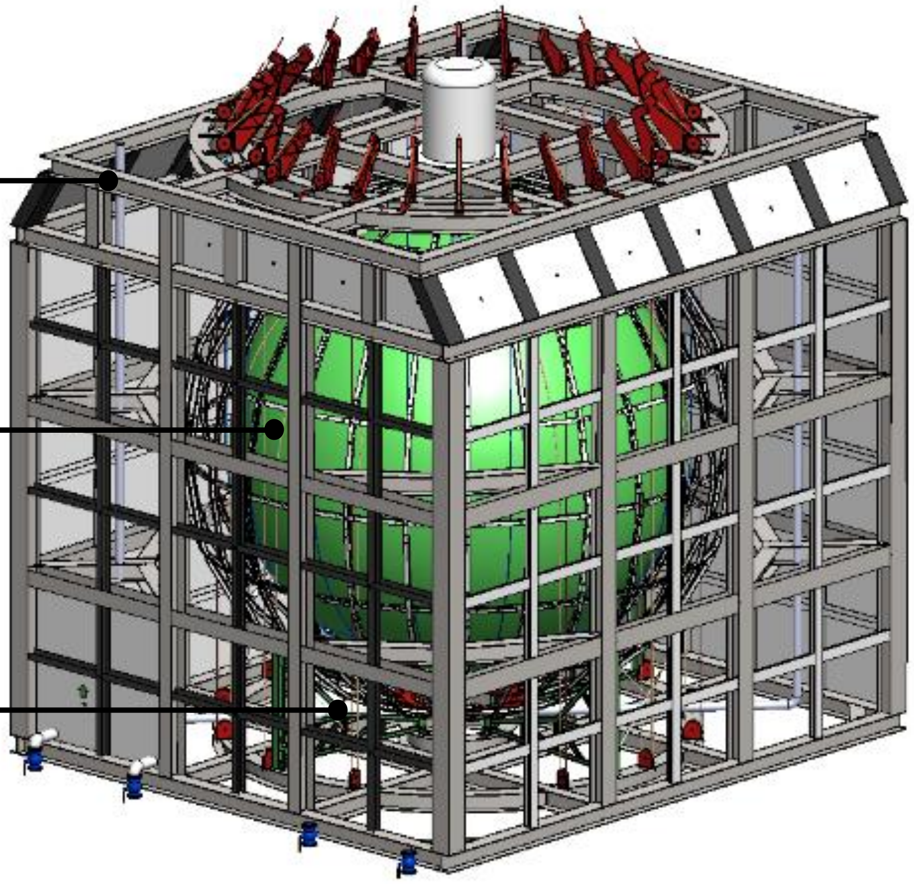

Project Overview

- Located in China Jingping Underground Laboratory
- Vertical rock overburden of approximately 2,400 meters
- Extremely low cosmic-ray flux and natural radioactive background

Detector structure

- Stainless steel frame and PMT supporting structure
- Acrylic vessel as the core container of the target medium
- Synthetic fiber rope system for support and positioning

01 Background

➢ 1.2 Jinping Neutrino Detector and the need for a rope-supported acrylic vessel

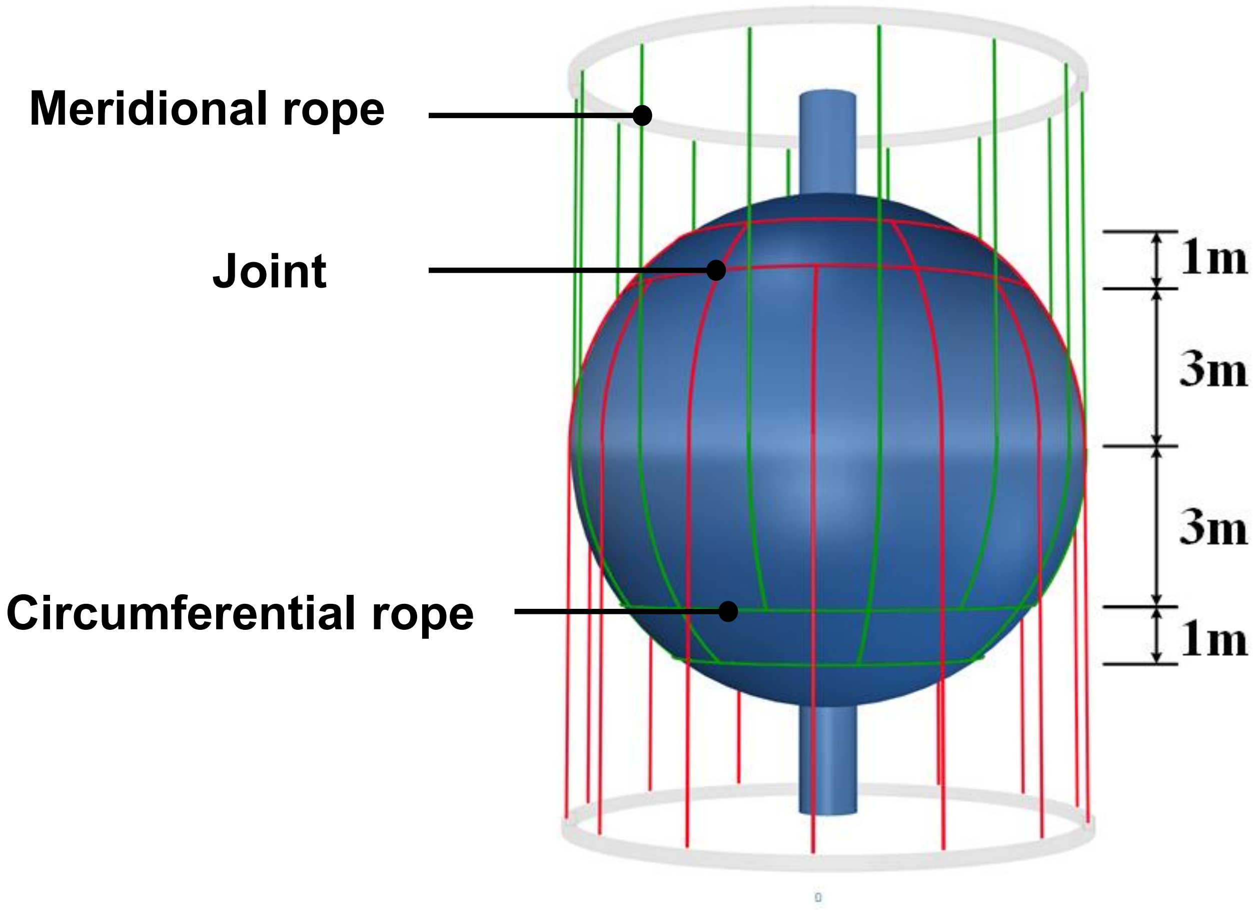

Fiber ropes system

- 28 meridional ropes are arranged, with 14 on each hemisphere.
- Circumferential ropes connect the meridional ropes to form the rope network.
- Loads are transferred to the surrounding steel structure.
- Rope length and initial tension can be adjusted during installation.

1.3 Key requirements and constraints for designing synthetic fiber rope support system

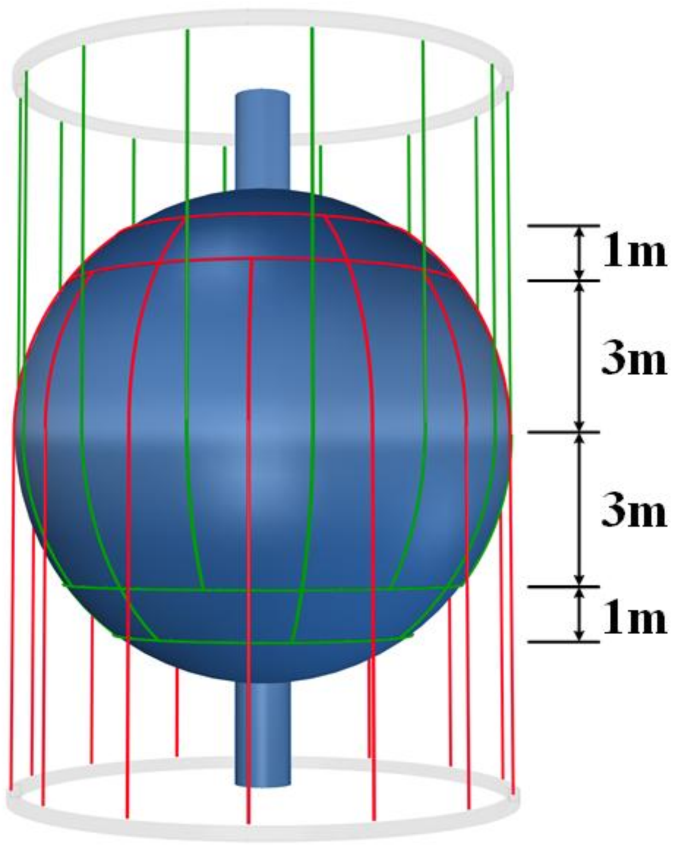

1. Long-term liquid immersion

Ropes must maintain stable performance in water- and oil-based liquid environments over long-term service.

2. Low radioactive background

Materials should minimize background interference with neutrino detection.

3. Low creep

Ropes must exhibit low creep because excessive long-term deformation could change the position of the acrylic vessel

4. High strength

Ropes must provide sufficient tensile capacity with a small cross section.

5. Joint reliability

Rope-joint connections should ensure safe and stable load transfer.

6. Adjustable installation

Rope length and initial tension should be adjustable during installation.

2

Selection of High-Performance Fiber Ropes

02 Selection of High-Performance Fiber Ropes

➢ 2.1 Elongation and Failure Behavior of High-Performance Fiber Ropes

Property	Technora	Vectran	JX99	C90
Fiber type	Aramid	LCP	HMPE	
Density g/cm^3	4.4	3.31	3.44	3.3
Creep tendency	low	low	High	low
ABS / kN	45.9	42.4	54.7	53.9

Specimen ID	Loading procedure	Objective
T1/V1/J1/C1	The fiber rope was subjected to three loading cycles at 50% of the estimated breaking load and was then loaded in tension to failure.	To determine the breaking load
T2/V2/J2/C2	Based on the breaking load obtained from specimen T1/V1/J1/C1, the fiber rope was subjected to three loading cycles at 50% of the measured breaking load. It was subsequently loaded stepwise to 1%, 4%, 8%, …, 48%, and 50% of the breaking load. The gauge length was measured at each loading level, after which the rope was loaded in tension to failure.	To determine the breaking load and tensile modulus
T3/V3/J3/C3		To determine the breaking load and tensile modulus
T4/V4/J4/C4		To determine the breaking load and tensile modulus

- **Before conducting the creep tests, monotonic tensile tests were performed on four types of 8 mm-diameter ropes to determine their tensile moduli and breaking loads.**

02 Selection of High-Performance Fiber Ropes

➢ 2.1 Elongation and Failure Behavior of High-Performance Fiber Ropes

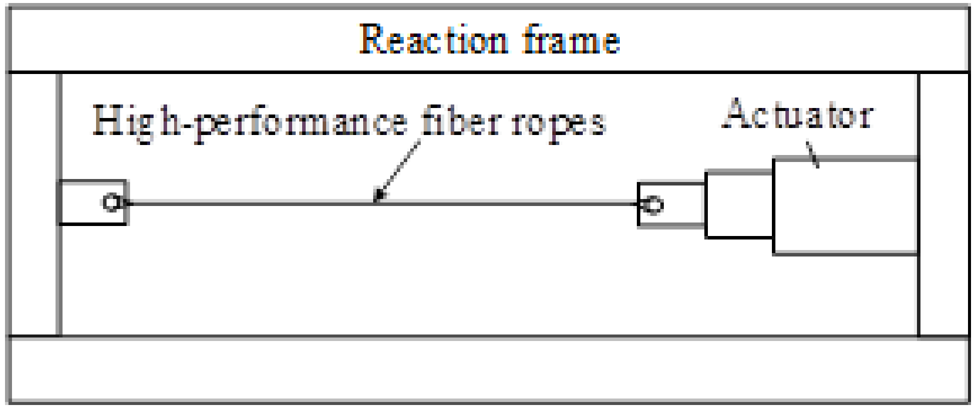

Test Configuration

- Four specimens were tested for each rope type.
- Eye-spliced terminations were fabricated at both ends for connection to the test apparatus.
- The unloaded eye-to-eye length of each specimen was approximately 2.2 m.

Average Breaking Load

- Technora: 45.9 kN Vectran: 42.4 kN
- JX99: 54.7 kN C90: 53.9 kN

The corresponding tensile moduli

- Technora: 11.91 Gpa Vectran: 15.22 Gpa
- JX99: 17.48 Gpa C90: 17.43 GPa

02 Selection of High-Performance Fiber Ropes

➢ 2.2 Creep test

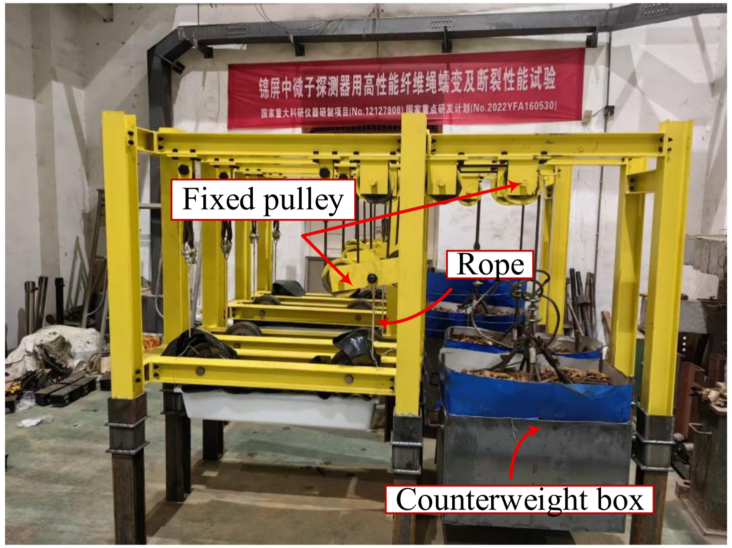

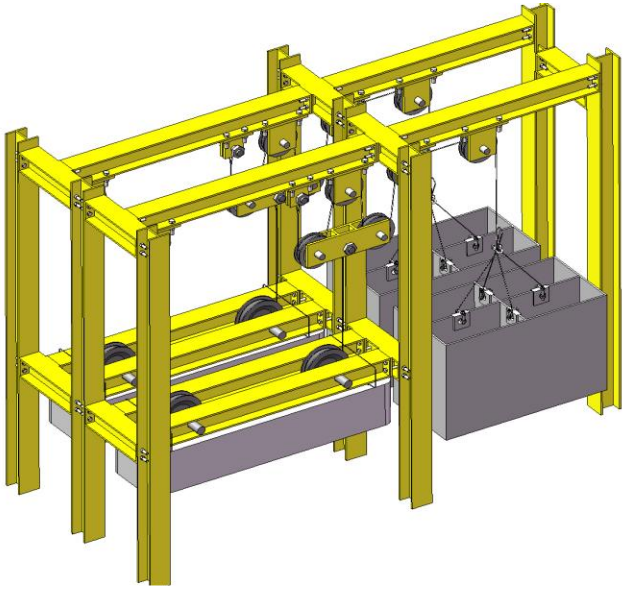

Test Conditions

- Rope types: Technora, Vectran, JX99 and C90
- Liquid environments: purified water and food-grade white oil
- Sustained load levels: 0.10,0.40,0.55,0.70 and 0.85 ABS
- The load level of 0.10 ABS represents the design service condition.
- The applied loads were determined from the average breaking loads obtained in the tensile tests.

02 Selection of High-Performance Fiber Ropes

➢ 2.3 Failure mode of ropes

Creep failure mode of the ropes.

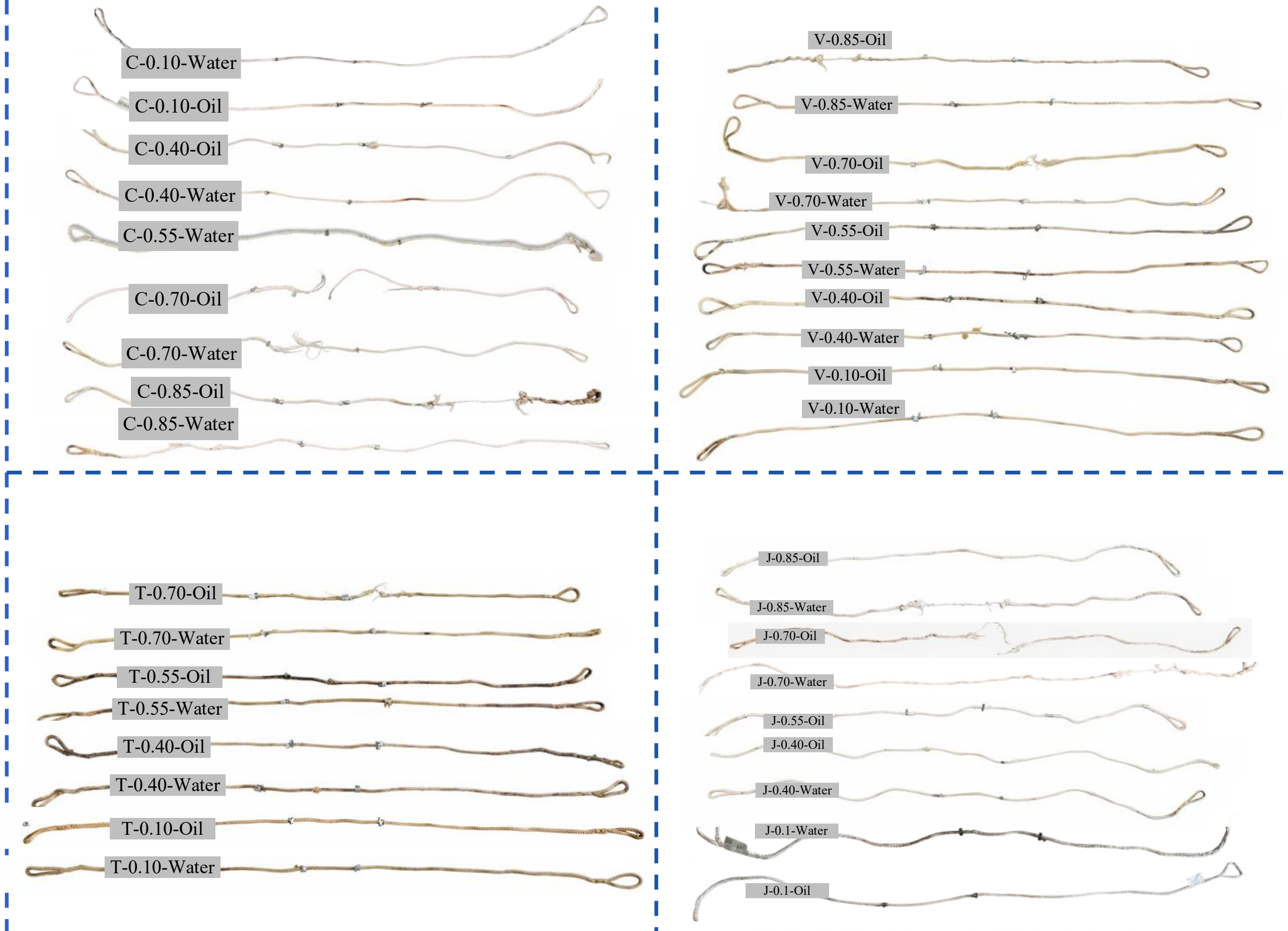

Failure Characteristics

- Rope morphology and failure mode were strongly dependent on the applied load level.
- Under low sustained loads, no macroscopic fracture was observed.
- The specimens mainly exhibited elongation and localized morphological changes.
- Under high sustained loads, fracture occurred in most specimens.
- Fiber-bundle separation and localized loosening were observed near some fracture regions.
- The results indicate progressive accumulation of long-term creep damage before final rupture.

02 Selection of High-Performance Fiber Ropes

➢ 2.4 Strain-time curves of ropes

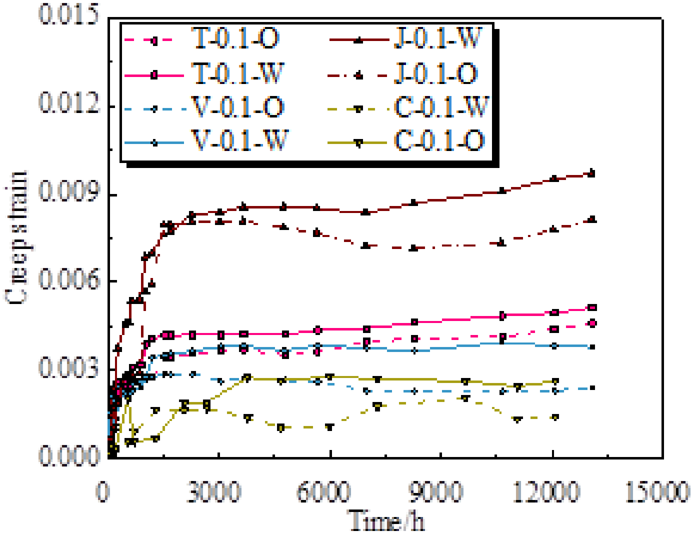

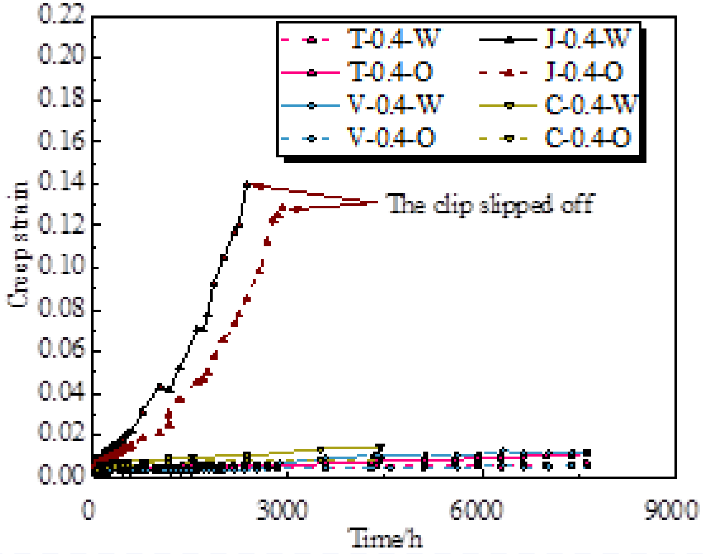

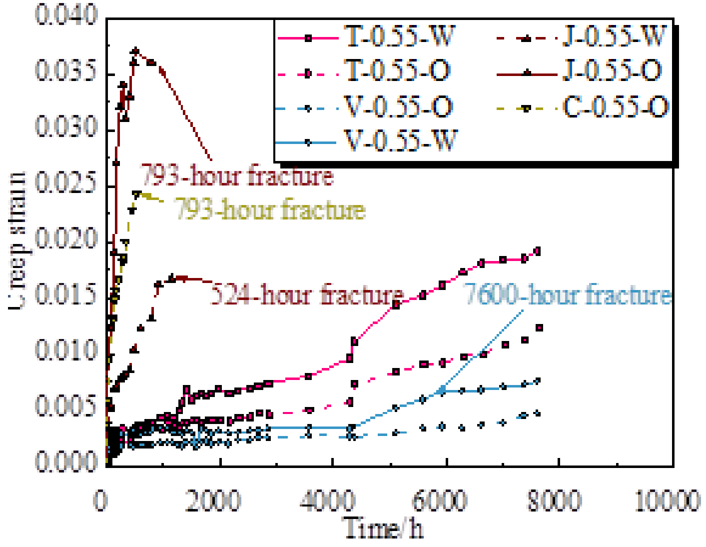

Creep Evolution

- All four ropes exhibited pronounced **time-dependent deformation** under sustained loading.
- At low load levels, the creep response consisted mainly of rapid primary creep followed by a slower secondary creep stage.
- No evident tertiary creep instability was observed under the **design load condition**.

Environmental and Material Effects

- Under the same condition, creep strain was **generally lower** in oil than in purified water.
- Technora and Vectran showed favorable creep resistance
- JX99 exhibited relatively **large creep deformation.**
- C90 showed the smallest creep deformation at **low and medium load levels.**

02 Selection of High-Performance Fiber Ropes

➢ 2.4 Strain-time curves of ropes

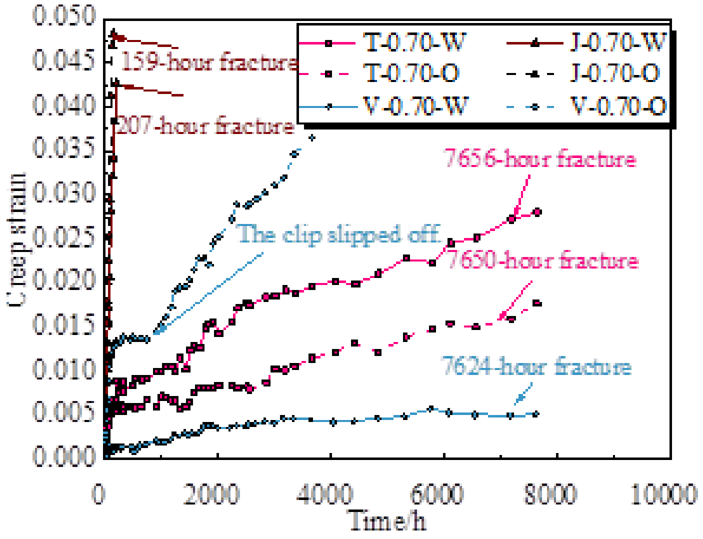

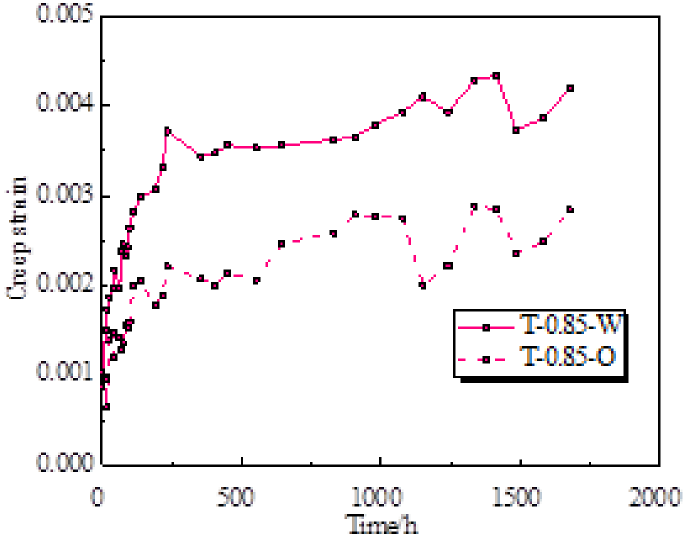

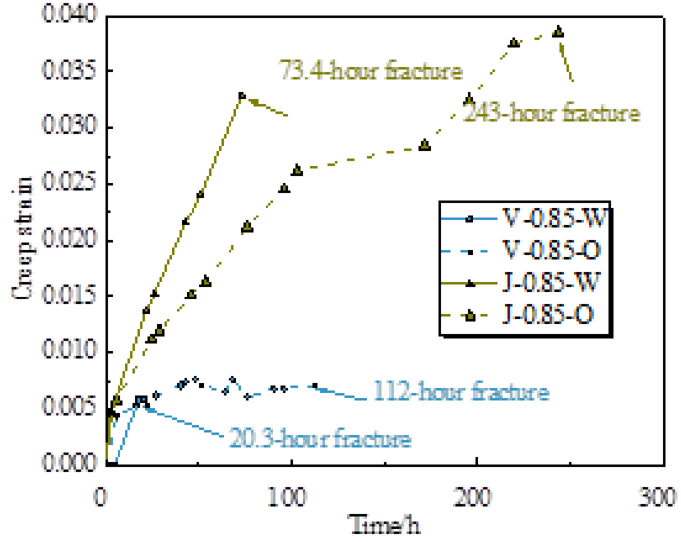

High-Load Creep Response

- At 0.70 and 0.85 ABS, both creep strain and creep rate increased significantly.
- Several specimens exhibited accelerated deformation in the later stage, corresponding to tertiary creep.
- Fiber-bundle separation, localized loosening and progressive damage were observed near the fracture regions.

Rupture Resistance

- Technora and Vectran exhibited the greatest rupture resistance under high sustained loads.
- JX99 exhibited substantial creep deformation and insufficient long-term creep stability.
- C90 showed relatively lower rupture resistance under high load levels

02 Selection of High-Performance Fiber Ropes

➤ 2.5 Creep test conclusions

III. Radionuclide Analysis

No.	Nuclide	Energy (keV)	A_u (mBq/kg)	MDA(mBq/kg)	A(mBq/kg)
1.	$^{210}Pb(^{223}U)$	46.539			570. 14±83. 36
2.	$^{226}Ra(^{238}U)$	186.211			577.15±130. 07
3.	$^{214}Pb(^{238}U)$	351.93			145. 42±18. 18. 28
4.	$^{214}Bi(^{238}U)$	609.32			101.81±17. 07
5.	$^{228}Ac(^{232}Th)$	911.20			197.24±36. 31
		968.97			150.24±46. 44
6.	$^{208}Tl(^{232}Th)$	583.188			99.21±11. 05
7.	^{40}K	1460.7			334. 24±107. 87
8.	^{137}Cs	661.66	16.42		
9.	^{60}Co	1173.23	15.68		
Measurement start time: 2023-10-17 08:51					
Measurement end time: 2023-10-22 08:51					
Live measurement time: 432000 s					

(1) Upper-limit activity (A_u): when the net count is lower than the decision limit L_C (i.e., the count is not significant), the activity is expressed as less than the upper-limit activity;

III. Radionuclide Analysis

No.	Nuclide	Energy (keV)	A_u (mBq/kg)	MDA(mBq/kg)	A(mBq/kg)
1.	$^{210}Pb(^{2238}U)$	46.539			162. 53±57. 45
2.	$^{226}Ra(^{238}U)$	186.211	88.53		
3.	$^{214}Pb(^{238}U)$	351.93			46. 94±11. 28
4.	$^{214}Bi(^{238}U)$	609.32			60.31±13. 71
5.	$^{228}Ac(^{232}Th)$	911.20	51.37		
		968.97	69.25		
6.	$^{208}Tl(^{232}Th)$	583.188		13.77	
7.	^{40}K	1460.7			1389. 94±182. 86
8.	^{137}Cs	661.66	6.47		
9.	^{60}Co	1173.23	8.74		
Measurement start time: 2023-10-12 08:45					
Measurement end time: 2023-10-17 08:45					
Live measurement time: 432000 s					

(1) Upper-limit activity (A_u): when the net count is lower than the decision limit L_c (i.e., the count is not significant), the activity is expressed as less than the upper-limit activity;

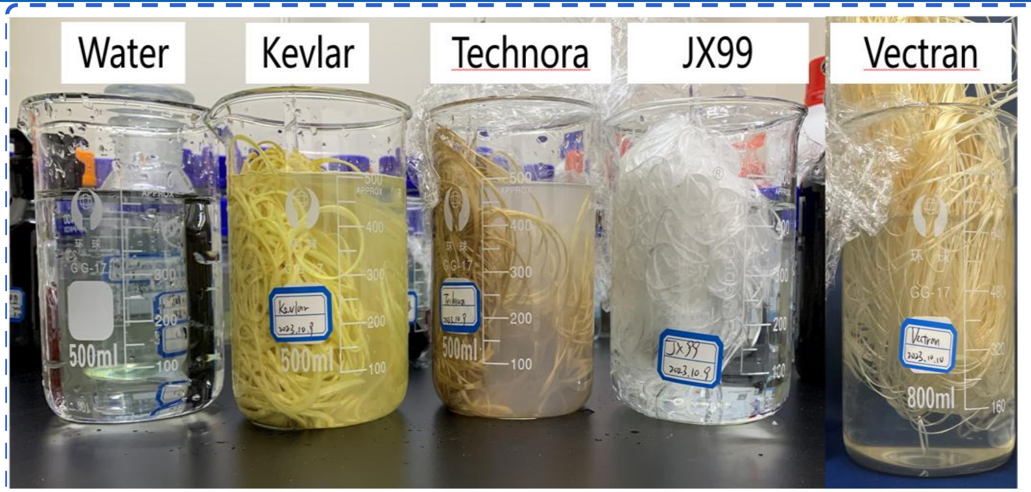

Based on the comprehensive test and characterization results, C90 was selected for the JNE rope support system!

3. Radionuclide Analysis

No.	Nuclide	Energy (keV)	A_u (mBq/kg)	MDA(mBq/kg)	A(mBq/kg)
1.	$^{210}Pb(^{2238}U)$	46.539			192. 27±52. 82
2.	$^{226}Ra(^{238}U)$	186.211	140.09		
3.	$^{214}Pb(^{238}U)$	351.93	---		
4.	$^{214}Bi(^{238}U)$	609.32	---		
5.	$^{228}Ac(^{232}Th)$	911.20	36.93		
		968.97	31.35		
6.	$^{208}Tl(^{232}Th)$	583.188	15.30		
7.	^{40}K	1460.7	256.26		
8.	^{137}Cs	661.66	5.04		
9.	^{60}Co	1173.23	9.60		
Measurement start time: 2024-01-12 08:49					
Measurement end time: 2024-01-19 08:49					
Live time: 604800 s					

(1) Upper limit activity (A_u): When the net count is less than the decision limit L_C (i.e., not statistically significant), the activity is reported as less than the upper limit activity;
(2) Minimum detectable activity (MDA): When the net count is greater than the decision limit L_C but less than the detection limit L_D, the activity is reported as less than the MDA;
(3) Activity (A): When the net count is greater than the detection limit L_D, the activity can be calculated.

JX99

3. Radionuclide Analysis

No.	Nuclide	Energy (keV)	A_u (mBq/kg)	MDA(mBq/kg)	A(mBq/kg)
1.	$^{210}Pb(^{2238}U)$	46.539			177. 03±53. 68
2.	$^{226}Ra(^{238}U)$	186.211			295.79±72. 28
3.	$^{214}Pb(^{238}U)$	351.93	---		
4.	$^{214}Bi(^{238}U)$	609.32	---		
5.	$^{228}Ac(^{232}Th)$	911.2	18.82		
6.	$^{208}Tl(^{232}Th)$	583.188	14.86		
7.	^{40}K	1460.7	237.38		
8.	^{137}Cs	661.66	4.51		
9.	^{60}Co	1173.23	7.99		
Measurement start time: 2024-07-22 15:15					
Measurement end time: 2024-07-29 15:15					
Live time: 604800 s					

(1) Upper limit activity (A_u): When the net count is less than the decision limit L_C (i.e., not statistically significant), the activity is reported as less than the upper limit activity;
(2) Minimum detectable activity (MDA): When the net count is greater than the decision limit L_C but less than the detection limit L_D, the activity is reported as less than the MDA;
(3) Activity (A): When the net count is greater than the detection limit L_D, the activity can be calculated.

C90

containing JX99 and C90 remained relatively **clear.**

- Gamma-radioactivity measurements also showed **significant differences** among the ropes. Vectran exhibited relatively **high activities** of several radionuclides from the uranium and thorium decay chains.
- By comparison, JX99 and C90 exhibited lower overall gamma-radioactivity levels.

➢ 2.6 Unified creep model: modeling concept

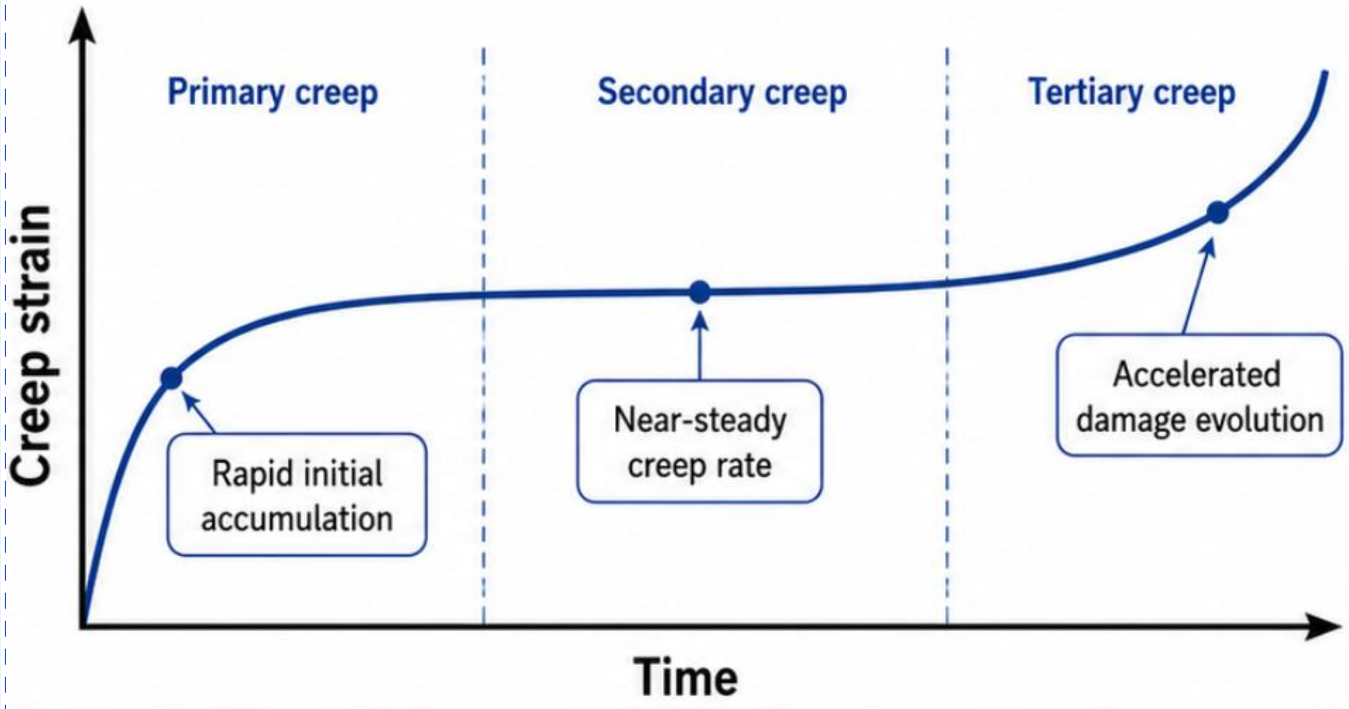

Creep response = primary creep + secondary creep
(+ tertiary creep for rupture cases)

Model Motivation

- **Existing models are commonly developed for a single material or service condition.**
- **A unified model is required to describe different rope types, liquid environments and load levels.**
- **Both non-rupture and creep-rupture responses need to be represented.**

Three-Stage Interpretation

Primary creep: rapid initial strain accumulation caused by internal adjustment.

Secondary creep: a relatively stable long-term creep rate.

Tertiary creep: accelerated damage evolution before rupture.

Unified Modeling Framework

- **Low and medium loads: primary creep + secondary creep**
- **High loads: primary creep + secondary creep + tertiary damage**
- **Main variables: rope type, liquid environment, sustained load level and time**

➢ 2.7 Unified creep model: constitutive equations

Non-rupture model

$$\varepsilon(t) = A\left(1 - e^{-\left(\frac{t}{\tau}\right)^{m}}\right) + \dot{\varepsilon}_s\, t$$

Applicable to low and medium load levels

- A: amplitude of primary creep
- τ: time scale of primary creep
- m: shape parameter of primary creep
- $\dot{\varepsilon}_s$: near-steady-state creep rate

Non-Rupture Model

- The first term describes the **primary creep stage**, in which strain increases rapidly and then gradually stabilizes.
- (A) controls the magnitude of primary creep, while τ and (m) determine its time scale and curve shape.
- The linear term $\dot{\varepsilon}_s$ represents the continuous strain accumulation during the secondary creep stage.
- The model contains no damage term and is therefore used for specimens **without** creep rupture.
- It is mainly applicable to the valid low- and medium-load cases below approximately 0.50

02 Selection of High-Performance Fiber Ropes

2.7 Unified creep model: constitutive equations

Rupture model

$$\varepsilon_R(t) = A\left(1 - e^{-\left(\frac{t}{\tau}\right)^m}\right) + \dot{\varepsilon}_s t + D\left[\frac{t - t_c}{t_f - t_c}\right]^q H(t - t_c)$$

$$t_c = \alpha(i) t_f$$

Applicable to high-load rupture cases

- D: amplitude of tertiary damage term
- t_f: characteristic life scale
- q: acceleration parameter
- $H(t - t_c)$: Heaviside function
- $\alpha(i)$: onset ratio of tertiary creep

Rupture Model

- The rupture model retains the primary and secondary creep terms of the non-rupture model.
- An additional delayed-onset damage term is introduced to describe the tertiary creep stage.
- The Heaviside function ($H(t-t_c)$) activates the damage term only after the onset time (t_c).
- (D) controls the magnitude of accelerated creep, while (t_f) represents the characteristic creep life.
- (q) controls the acceleration rate of tertiary creep.
- The onset time is defined as $t_c = \alpha(i)t_f$, where $\alpha(i)$ accounts for the effect of rope type.
- This model is used for high-load cases exhibiting accelerated deformation and eventual rupture.

02 Selection of High-Performance Fiber Ropes

➢ 2.8 Unified creep model: Parameterization and Predictive Capability

Fitted parameter expressions

Non-rupture model parameters:

$$\ln A = -3.55 - 1.45\lambda - 0.44\,z - 2.05\,I_V - 0.58\,I_H - 0.74\,I_C - 2.41\,\lambda\,I_V - 1.04\,\lambda\,I_H + 2.59\,\lambda\,I_C$$

$$\ln \tau = 16.90 - 13.13\,\lambda - 1.69\,z - 11.60\,I_V - 7.17\,I_H - 1.05\,I_C - 18.30\,\lambda\,I_V - 0.79\,\lambda\,I_H - 5.38\,\lambda\,I_C$$

$$\ln \dot{\varepsilon}_s = -29.06 + 6.73\lambda - 4.83\,z - 1.83\lambda\,z - 0.87\,I_V - 1.97\,I_H + 7.27\,I_C$$

$$m(i) = \exp(-1.41 + 0.39\,I_V + 0.72\,I_H + 0.50\,I_C)$$

Rupture model parameters:

$$\ln D = -15.25 + 23.87\lambda - 0.36\,z + 15.30\,I_V - 27.13\lambda\,I_V$$

$$\ln t_f = 1.15 + 14.38\,\lambda + 0.30\,z + 7.93\,I_V - 13.38\,\lambda\,I_V$$

$$\alpha(i) = \frac{1}{1 + \exp\left(-(-17.53 + 16.60\,I_V)\right)}$$

Technora is taken as the reference rope type.

Prediction accuracy

Rope type	MRE / %	RMSE / $\times 10^{-3}$	R^2
Technora	12.1	1.32	0.951
Vectran	10.6	0.86	0.964
JX99	13.8	1.05	0.942
C90	11.9	0.94	0.948
Mean	**12.1**	**1.04**	**0.951**

Main findings

- The model reproduced the primary and secondary creep stages well.
- Accelerated tertiary creep under high loads was captured reasonably.
- The overall coefficient of determination was approximately 0.95.
- The model provides a basis for creep prediction and material selection.
- Variables considered include load level, liquid environment, and rope type.

3

Full-Scale Tensile Tests of C90 Fiber Ropes

03 Full-Scale Tensile Tests of C90 Fiber Ropes

➢ 3.1 Specimen Configuration and Test Setup

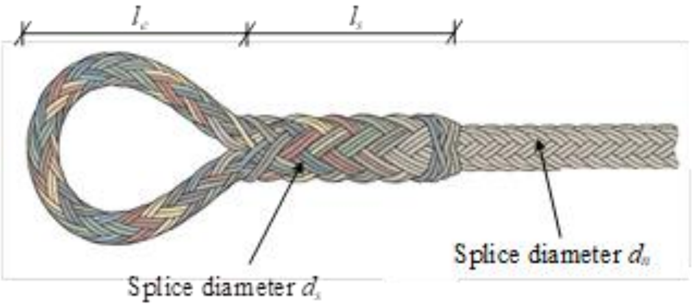

Specimen Types	d_n/mm	d_s/mm	l_n/mm	l_s/mm	l_e/mm
Meridional ropes	40.33	46.75	50	1610	510
Circumferential ropes	46.67	54.14	50	1895	560

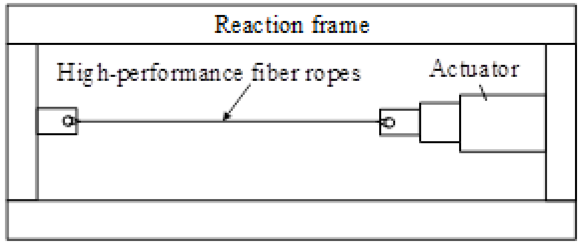

Preliminary breaking test

- 3 cycles at 50% of the estimated breaking load.
- Monotonic loading to failure

Bedding-in cycles

- 3 cycles at 50% of the measured breaking load.

Stepwise loading

- 1%, 4%, 8%,……,48%,50% of the breaking strength.

03 Full-Scale Tensile Tests of C90 Fiber Ropes

➢ 3.2 Tensile results and failure mode

Failure Characteristics

- Neither rope exhibited a clean and instantaneous fracture across the entire cross-section.
- Pronounced fiber-bundle loosening and local filament drawing were observed.
- The final failure developed progressively through successive rupture of the internal fiber bundles.

Failure Mechanism

- Local damage initiated in highly stressed fiber bundles.
- The tensile force was continuously redistributed among the remaining strands.
- Damage accumulation and progressive strand rupture eventually caused the loss of the overall load-carrying capacity.

Engineering Interpretation

- Both meridional and circumferential ropes exhibited progressive rather than purely brittle failure.
- The braided configuration provided a certain degree of internal load redistribution before final rupture.
- The observed failure modes provide a physical basis for interpreting the nonlinear tensile response.

03 Full-Scale Tensile Tests of C90 Fiber Ropes

➢ 3.2 Tensile results and failure mode

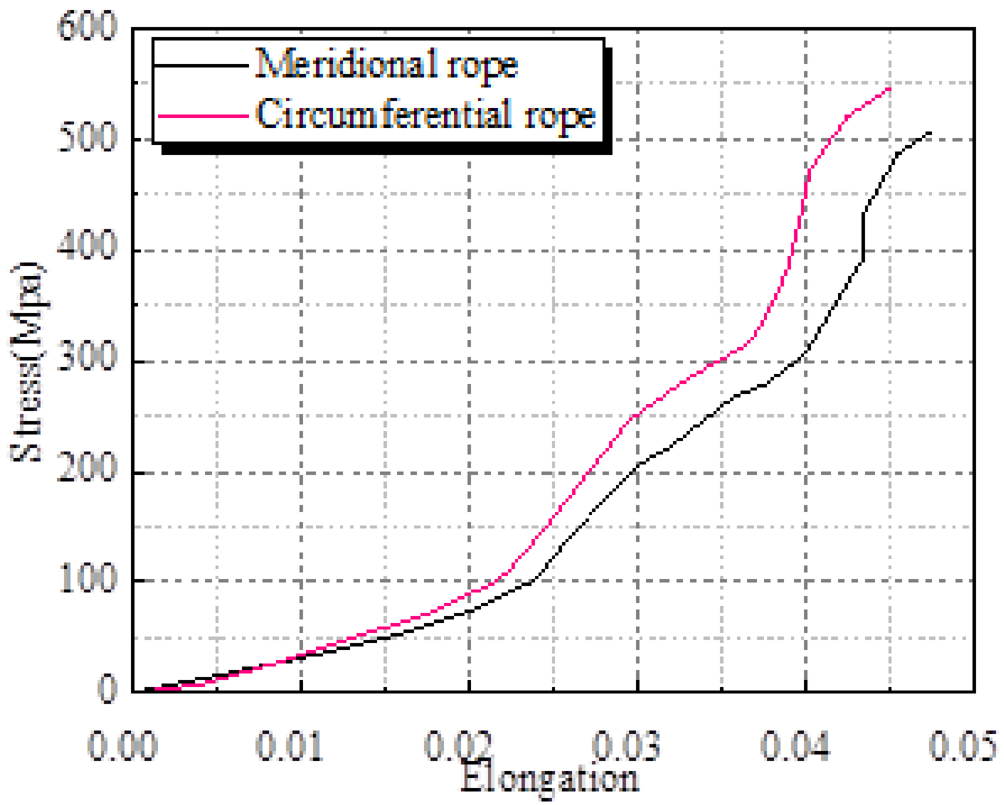

Mechanical properties

Property	Meridional rope	Circumferential rope
Nominal diameter / mm	40.33	46.67
Initial nominal area / mm²	1277.45	1710.66
Apparent tensile modulus / GPa	8.68	10.81
Axial stiffness / kN	11090	18500

Key observations

- Both rope directions showed stable nonlinear tensile responses.
- The circumferential rope exhibited higher axial stiffness owing to its larger diameter and area.
- The 1–3% elongation interval was used to evaluate the apparent tensile modulus.
- The measured parameters were used in the subsequent FE analysis and structural design.

03 Full-Scale Tensile Tests of C90 Fiber Ropes

➢ 3.3 Equivalent 12-Strand FE Modeling Strategy

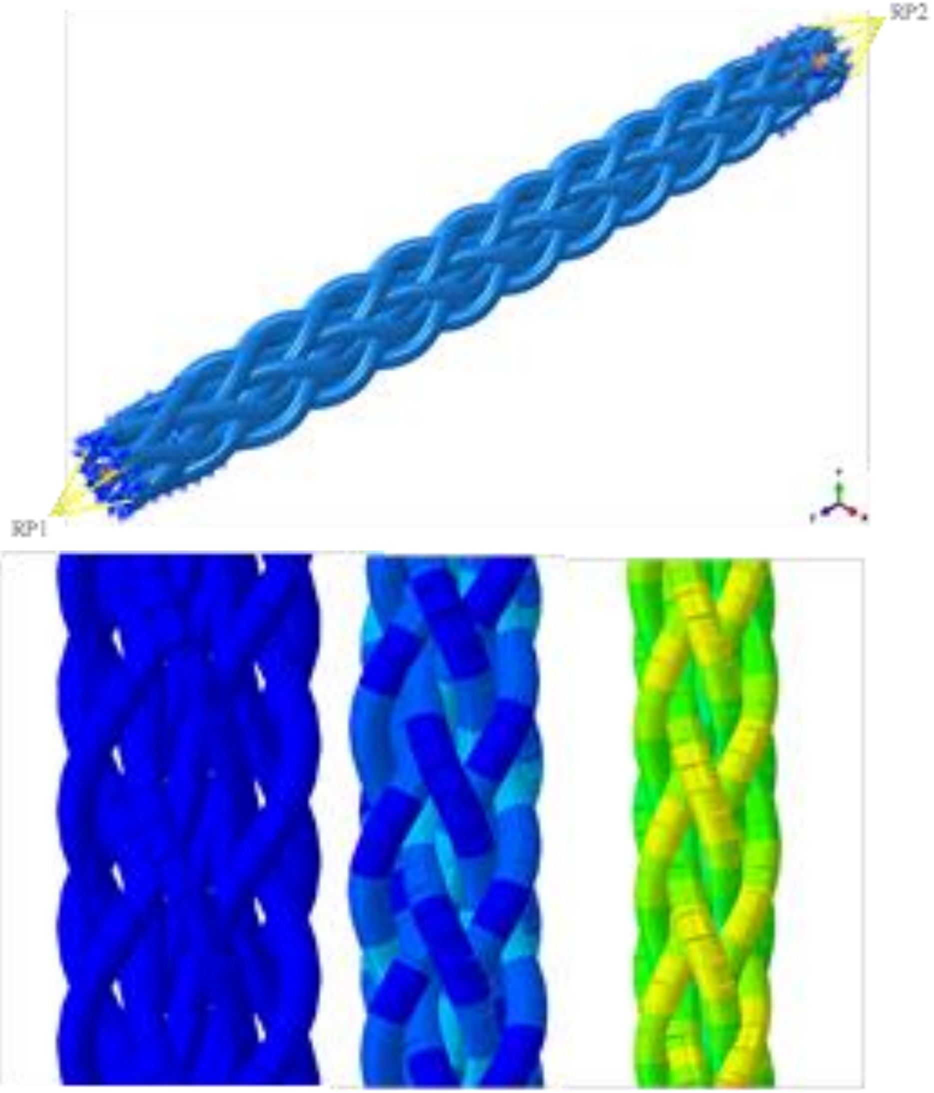

FE Modeling Strategy

- A 12-strand equivalent rope model was established to represent the braided C90 rope.
- Each strand was modeled using beam elements to capture the global tensile response.
- The model reproduces the overall rope geometry and strand interaction pattern.

Contact and Material Assumptions

- Hard contact was applied in the normal direction, while penalty friction with a coefficient of 0.10 was used in the tangential direction.
- Equivalent linear-elastic properties were assigned to the strands.

03 Full-Scale Tensile Tests of C90 Fiber Ropes

3.4 Validation of FE model

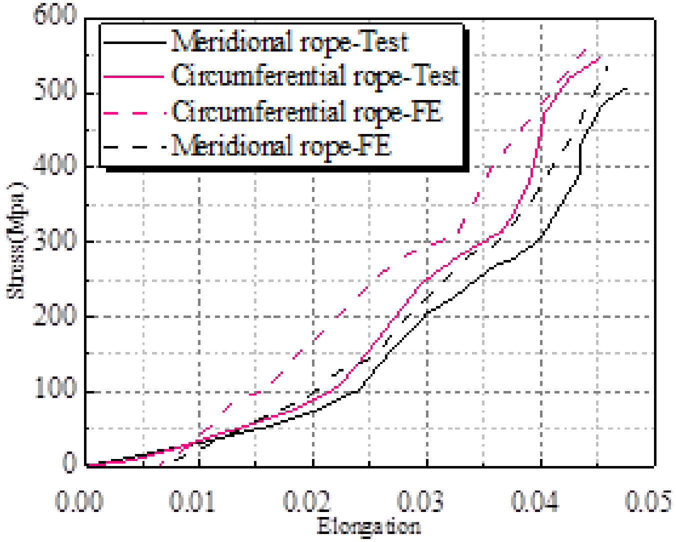

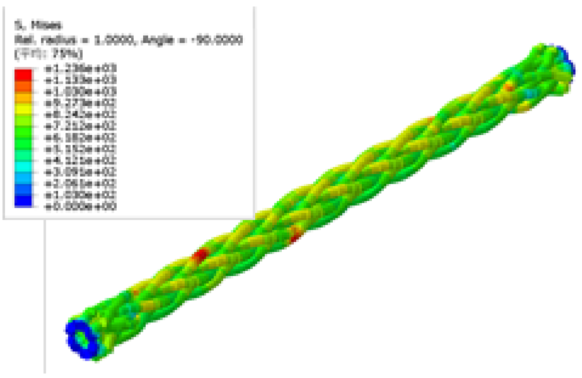

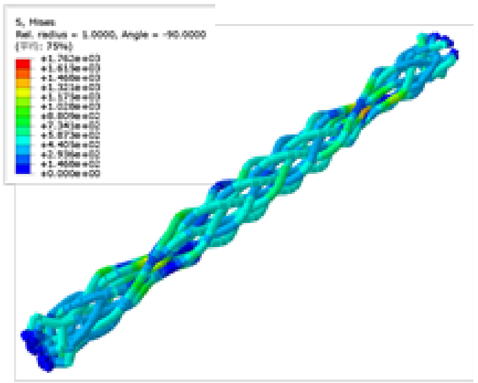

Rope type	Peak stress error / %	Peak elongation error / %	MAE / MPa	RMSE / MPa	NRMSE / %
Meridional rope	5.69	3.35	34.14	40.25	7.95
Circumferential rope	3.97	1.79	62.28	70.04	12.81
Mean	4.83	2.57	47.72	56.62	10.75

Key observations

- The FE model reasonably captured the overall nonlinear tensile response of both ropes.
- The predicted peak stress errors were 5.69% and 3.97% for the meridional and circumferential ropes, respectively.
- The corresponding peak elongation errors were 3.35% and 1.79%.
- The mean NRMSE was 10.75%, indicating satisfactory predictive accuracy.
- A local deviation was observed for the circumferential rope at elongations of 0.03–0.04, mainly due to inter-strand compaction, slippage and cross-sectional changes not explicitly modeled.

4

Joint Properties Of C90 Fiber Ropes

04 Joint Properties Of C90 High-performance Fiber Ropes

➢ 4.1 Joint test

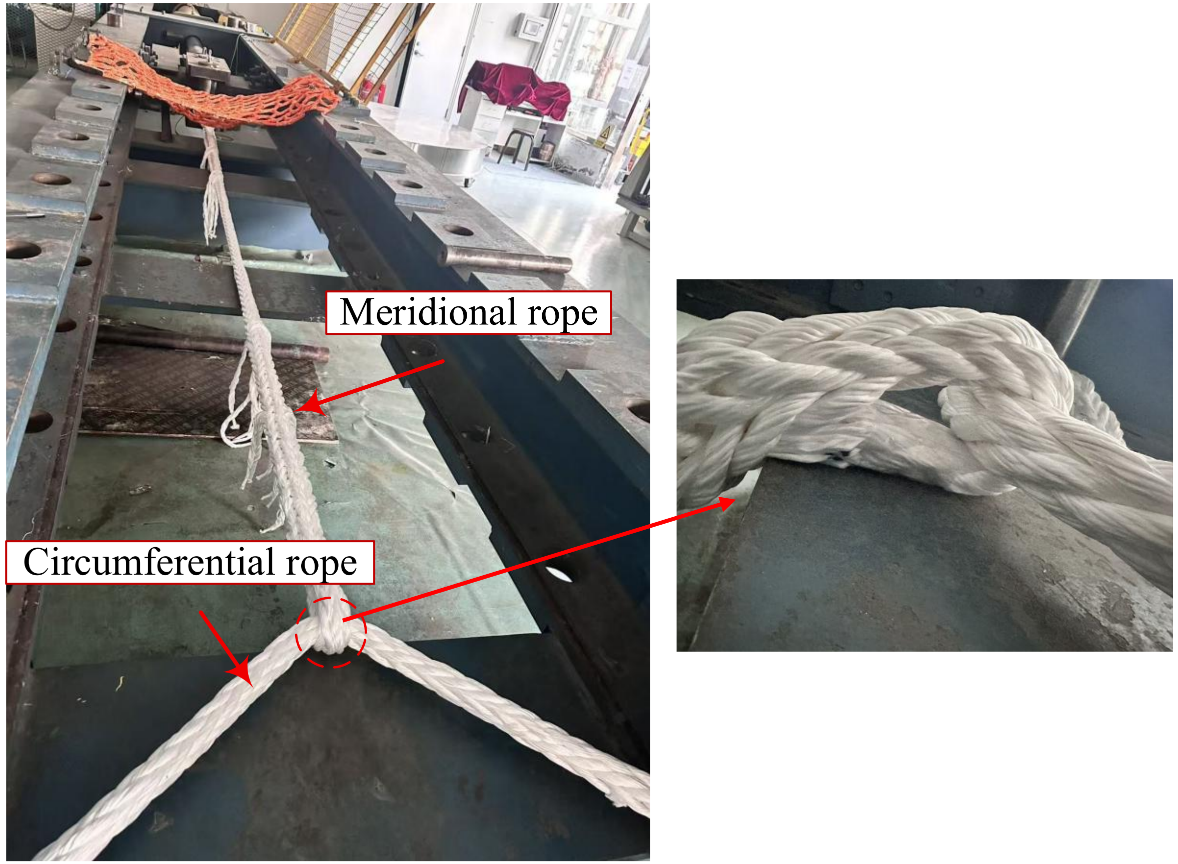

Specimen configuration

- One meridional rope and one circumferential rope were assembled into a representative engineering joint.
- The circumferential rope passed through the eye splice formed at the end of the meridional rope.
- The joint configuration reproduced the practical rope connection used in the support system.

Loading protocol

- The specimen was preloaded three times at 50% of the design reference load.
- It was then monotonically loaded to failure.
- Force, displacement and joint angle variation were recorded during the test.

04 Joint Properties Of C90 High-performance Fiber Ropes

➢ 4.2 Test result

Failure mode

Configurational change

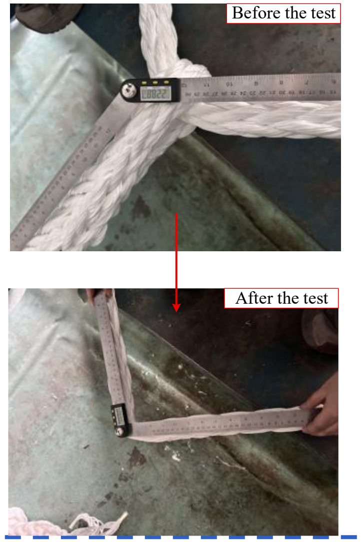

Load-displacement curve

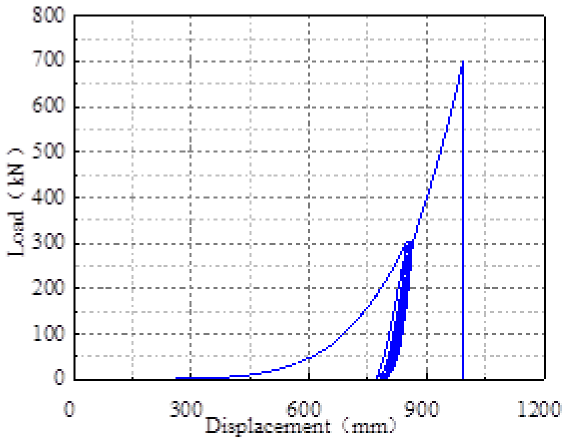

Failure characteristics

- Failure occurred in the meridional rope near the connection region.
- Progressive fiber-bundle rupture and local loosening were observed.
- The circumferential rope remained intact during the test.

Configurational response

- The included angle of the circumferential rope decreased during loading.
- Mean joint angle changed from 97.6° before loading to 95.1° at failure.
- The total angle reduction was about 2.5°.

Mechanical performance

- The load-displacement curve shows nonlinear tensile behavior.
- The measured joint failure load was about 700 kN.The corresponding strength utilization was about 81.4% of the meridional rope breaking load.

5

Rope Adjustment Device

05 Rope Adjustment Device

➢ 5.1 Schematic diagram and layout drawing of the rope adjustment device

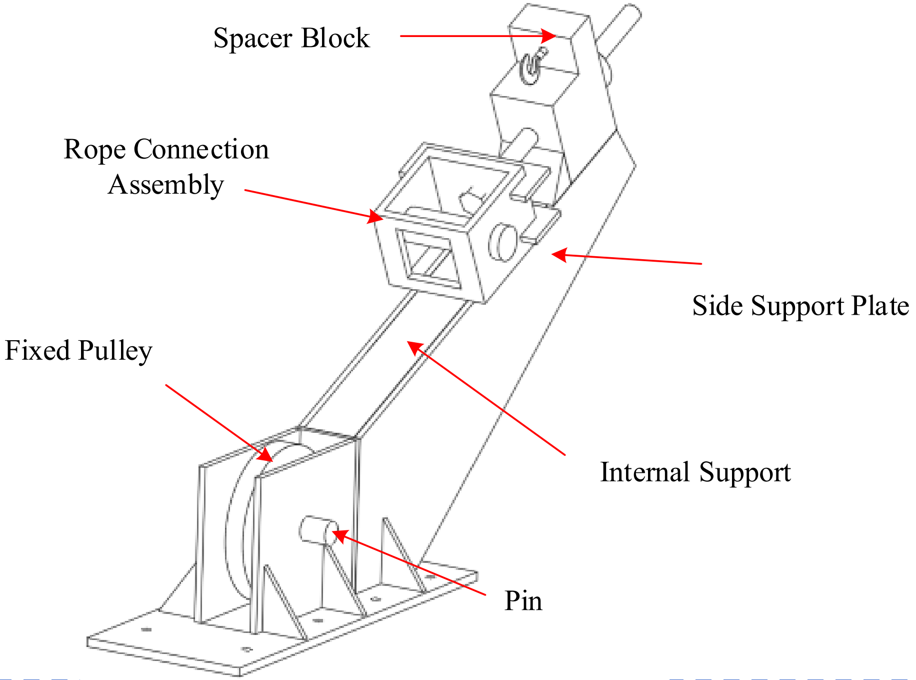

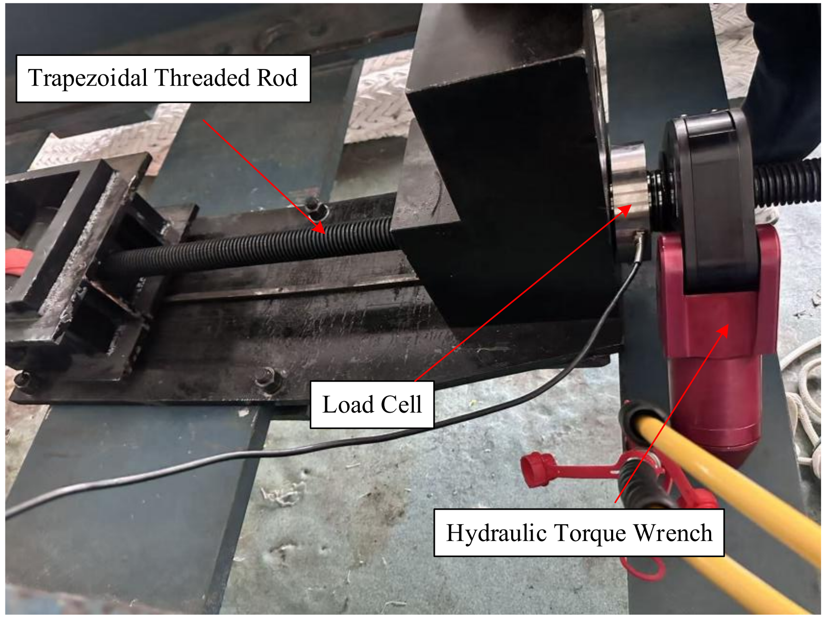

- **During installation, the rope length and initial tension must be controlled accurately.**
- **The proposed adjustment system uses a mechanical assembly that allows the rope position to be changed through bolt adjustment.**

- **All plates are 16 mm thick.**
- **The fixed pulley has an outer diameter of 360 mm and an inner diameter of 280 mm.**
- **The trapezoidal lead screw is 1 m long.**

05 Rope Adjustment Device

➢ 5.1 Schematic diagram and layout drawing of the rope adjustment device

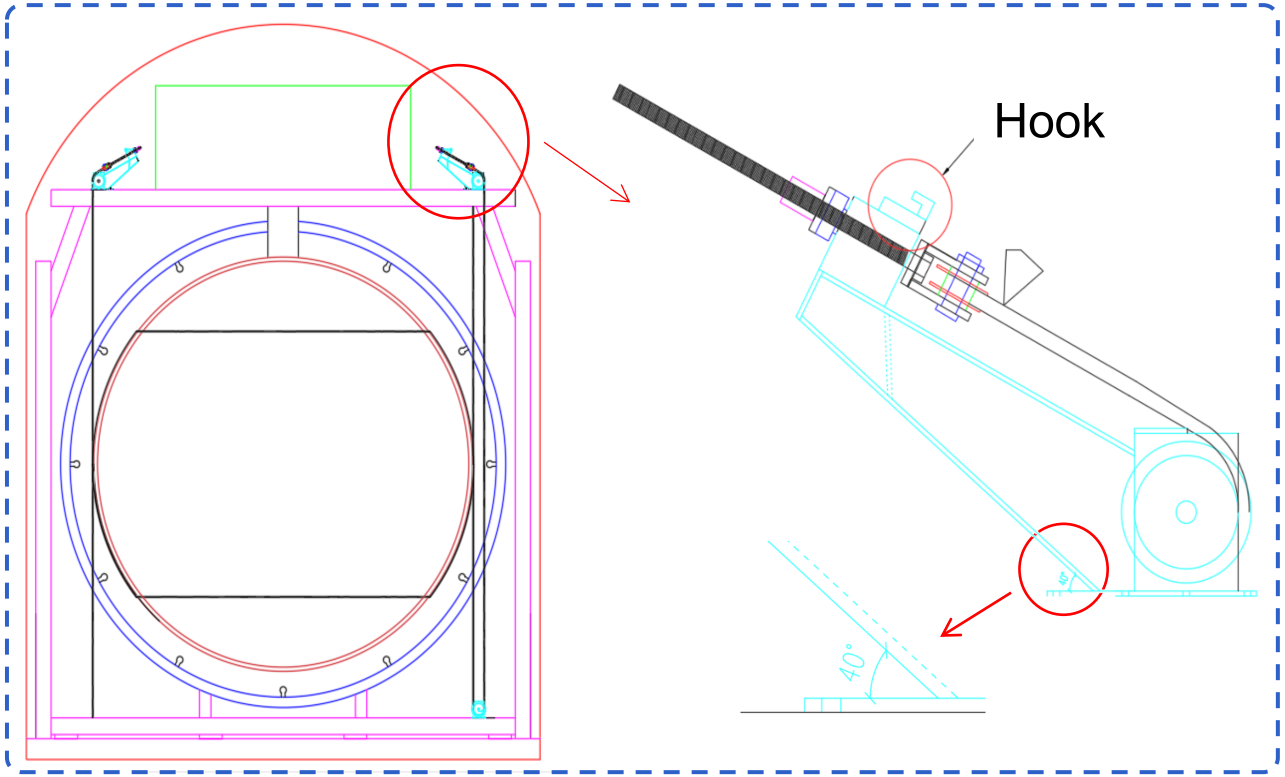

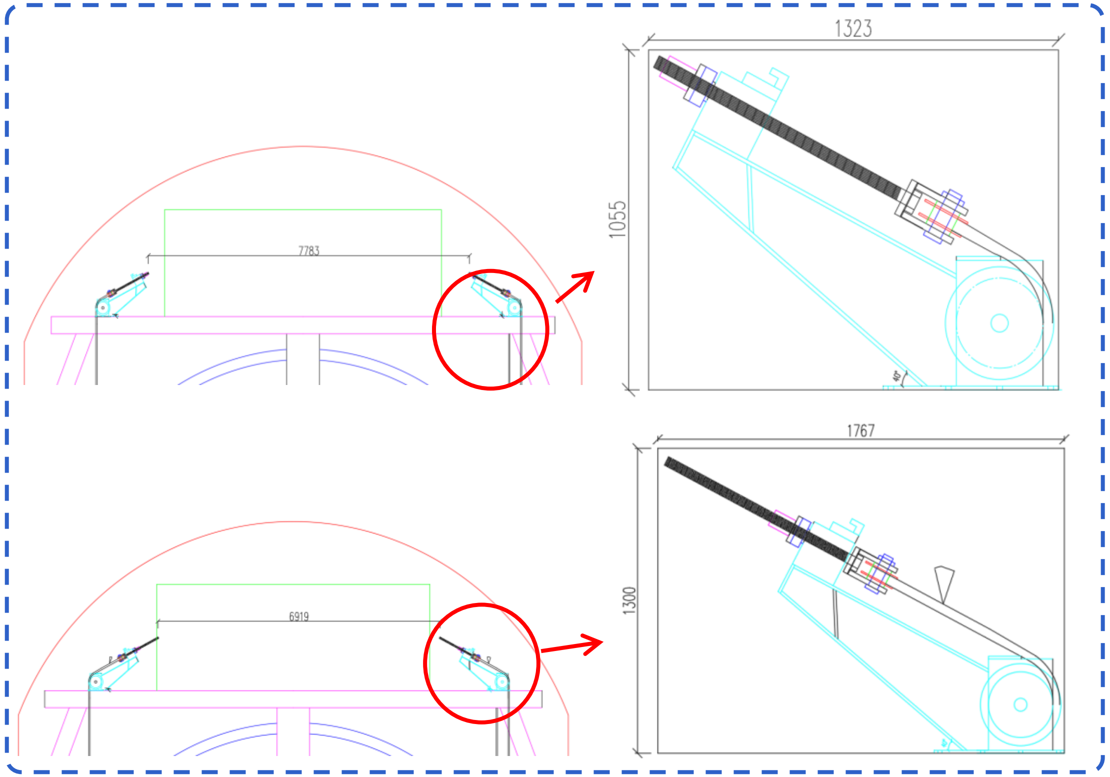

- The bolts are adjusted using a hydraulic wrench to enable installation and adjustment of the rope.
- Real-time tension monitoring is performed by pressure sensors located beneath the bolts.

05 Rope Adjustment Device

➢ 5.2 Safety verification via FE model

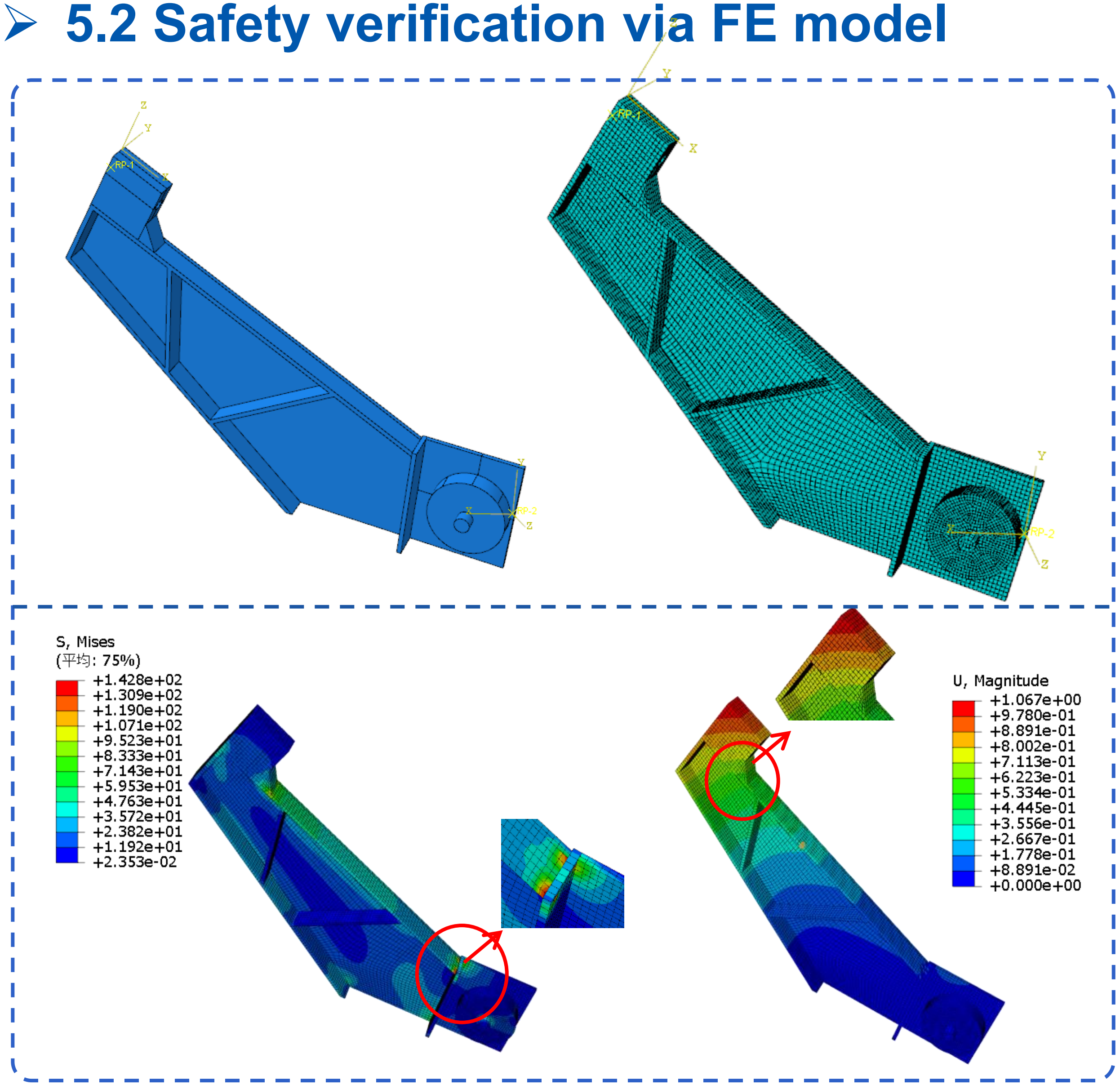

- **Finite element analysis was used to evaluate the adjustment device under the design loading condition.**

Key results

- **Maximum von Mises stress: 142.8 Mpa**
- **Maximum displacement: 1.07 mm**
- **Peak stress occurred near the local connection and geometric transition.**
- **Maximum displacement was observed at the loaded end of the device.**
- **The remaining regions exhibited relatively uniform and low stress levels.**

05 Rope Adjustment Device

➢ 5.2 Safety verification via FE model

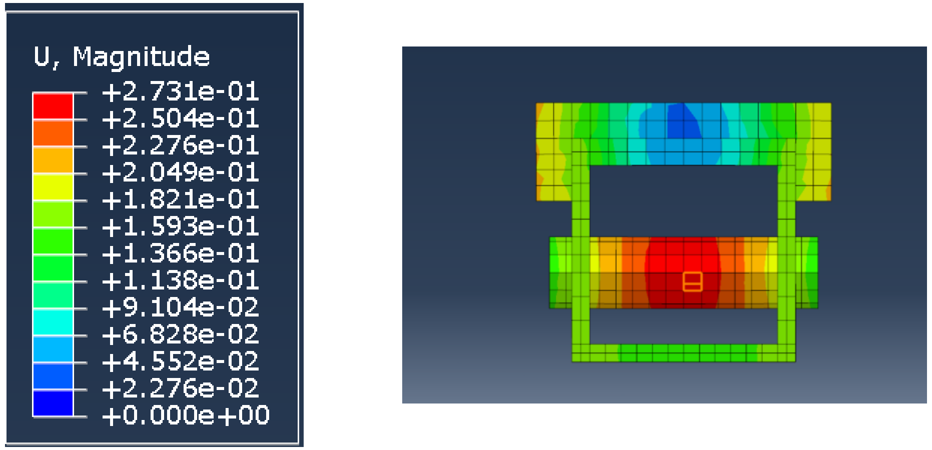

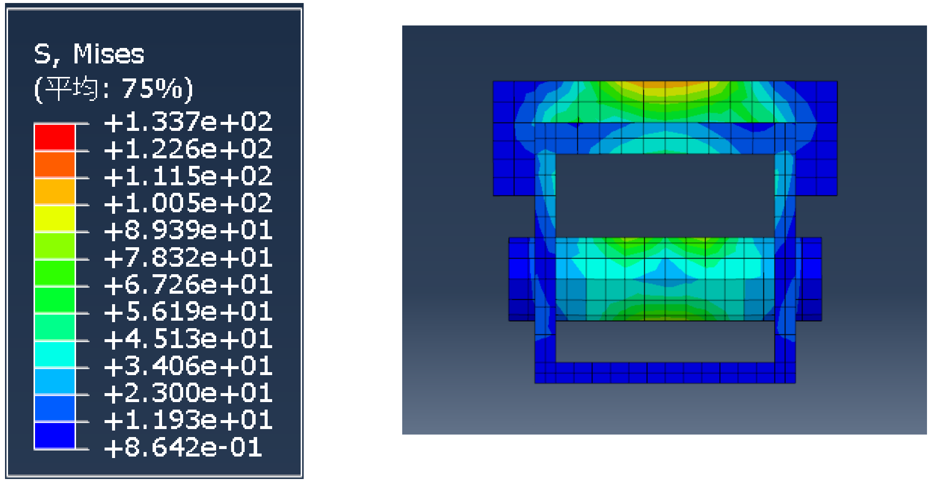

To prevent excessive axial force in the lead screw from causing deformation of the plates, a FE analysis was conducted for the rope connection device under the most unfavorable loading condition.

The results showed that

- **Both the overall deformation and stress were relatively small.**
- **The maximum deformation was 2.73 mm, occurring at the connection between the pin and the rope.**
- **The maximum von Mises stress was 133.7 MPa.**

□ **The FE results show that both the stress and deformation satisfy the engineering requirements!**

Conclusions

1. Rope Selection

C90 was selected based on its low creep deformation, good liquid compatibility, and low radioactive background.

2. Creep Prediction

A unified creep model was developed to describe primary, secondary, and tertiary creep under different loads and environments.

3. Full-Scale Rope Performance

Full-scale tensile tests confirmed the mechanical properties and progressive failure behavior of C90 ropes.

4. Joint and Device Verification

The rope joint and adjustment device showed sufficient load-bearing capacity, deformation control, and engineering applicability.

"Mechanical evaluation of high-performance fiber ropes: creep test, tensile response and joint behavior"

Thank you for your attention！